Heterogeneous and rate-dependent streptavidin-biotin unbinding revealed by high-speed force spectroscopy and molecular dynamics simulations

Felix Rico[1‡*], Andreas Russek[2‡], Laura González[3], Helmut Grubmüller[2*], and Simon Scheuring[4,5*]

[1] LAI U1067, Aix Marseille Univ, INSERM, CNRS, 163 avenue de Luminy, 13009 Marseille, France
[2] Department of Theoretical and Computational Biophysics, Am Faßberg 11, Göttingen, Germany
[3] Bioelectronics Group, Department of Electronics, Universitat de Barcelona, c/ Marti Franques 1, 08028 Barcelona, Spain
[4] Department of Anesthesiology, Weill Cornell Medical College, 1300 York Ave, New York, NY 10065, USA
[5] Departments of Physiology and Biophysics, Weill Cornell Medical College, 1300 York Ave, New York, NY 10065, USA

* Corresponding authors
‡ Equal contribution

Abstract

Receptor-ligand interactions are essential for biological function and their binding strength is commonly explained in terms of static lock-and-key models based on molecular complementarity. However, detailed information of the full unbinding pathway is commonly lacking due, in part, to the static nature of atomic structures and ensemble averaging inherent to bulk biophysics approaches. Here we combine molecular dynamics and high-speed force spectroscopy on the streptavidin-biotin complex to determine the binding strength and unbinding pathways over the widest dynamic range. Experiment and simulation show excellent agreement at overlapping velocities and provided evidence of the unbinding mechanisms. During unbinding, biotin crosses multiple energy barriers and visits various intermediate states far from the binding pocket while streptavidin undergoes transient induced fits, all varying with loading rate. This multistate process slows down the transition to the unbound state and favors rebinding, thus explaining the long lifetime of the complex. We provide an atomistic, dynamic picture of the unbinding process, suggesting that the lock-and-key mechanism may need revision in terms of many routes to the lock that might be relevant for other receptor-ligand bonds.

Text

Receptor/ligand bonds are at the core of almost every biological process. The lock-and-key model including eventual conformational changes is commonly accepted to describe the affinities and kinetic rates of receptor/ligand complexes, and is mainly based on molecular complementarity pictures from static structural data [1, 2]. Over the past decades, an impressive amount of knowledge has been accumulated on the structural and energetic determinants of bound states, thus enabling the increasingly successful rational design of nano-molar binders for therapy as well as the quantitative prediction of binding processes and free energies from atomistic simulations [3]. While protein folding and unfolding are thought to follow a multiplicity of pathways, the very mechanism of binding or unbinding of receptor/ligand complexes remains less investigated and is generally viewed by the simple lock-and-key model. Moreover, little is known on how the (un)binding dynamics is governed by the underlying microscopic processes - despite being key to a quantitative understanding of receptor-ligand complexes. Progress is mostly hampered by the lack of structural and thermodynamic information of the transient ligand/receptor conformations during unbinding, even for extensively studied systems such the complex formed by streptavidin (SA) and the small molecule biotin (b, vitamin H), one of the strongest non-covalent bonds known in nature.

Streptavidin forms the biotin-binding pocket with an eight-stranded, antiparallel beta-barrel capped by loop 3-4 (Fig. 1). In the native, tetrameric SA form, loop 7-8 from an adjacent monomer provides a closing lid to the pocket [4]. Biotin binds by forming an intricate and extensive network of hydrogen bonds with polar residues of SA [4, 5]. Its high affinity ($K_D \sim 10^{-13}$ M) and long lifetime ($\tau \sim 10$ days, $k_{\text{off}} \sim 10^{-6}$ s^{-1}) [6, 7, 8, 9], makes the SA/b system extensively used in biotechnology and biophysics. Dynamic forced disruption of the streptavidin-biotin complex by atomic force microscopy (AFM) and other techniques pioneered single molecule biomechanics [10, 11, 12]. [13] and provided estimates of the distance x_β to the unbinding transition state and the intrinsic bond lifetime [13, 14, 15]. Despite its seeming simplicity, AFM [11, 16, 17, 18, 19], optical tweezers [20], and biomembrane force probe [10, 21] experiments of streptavidin/biotin unbinding have reported dissimilar results suggesting an impressive complexity and heterogeneity in the unbinding pathway. Furthermore, these results were incompatible with ensemble bond-lifetime measurements.

Although recent experimental developments accessing the microsecond timescale have shed light into the complexity of single molecule transition paths of protein and nucleic acid (un)folding [22, 23, 24, 25], the amount of transient structural information extracted from single molecule experiments is rather limited. Therefore, most structural knowledge on unbinding/unfolding processes has been derived from atomistic simulations that were often limited to short time-scales inaccessible to experiments and therefore not rigorously validated [26, 27, 28]. Thus today, a direct relationship between the energy landscape and the dynamic structural details of these seemingly simple biomolecular processes is missing. As a result, it is still unclear (a) how biotin precisely outlives days and unbinds under load, (b) how and where biotin is located at the point of rupture and how the respective intermediates are stabilized, (c) if there is only one or possibly several unbinding pathways, and if so, (d) to what extent the unbinding path changes with loading rate and influences the binding capacity. Here we address these questions by combining high-speed force spectroscopy (HS-FS) and full atomistic simulations to observe biotin unbinding from streptavidin over eleven orders of magnitude of loading rates. We show that the unbinding pathway of the small molecule biotin from SA is much more complex than a "key that leaves a lock" but implicates a multitude of pathways and intermediate binding sites far from the binding pocket, much alike protein unfolding has various pathways and intermediate folding states.

HS-FS experiments used microcantilevers coated with biotin to probe the force required to rupture individual SA-b bonds at various loading rates (**Fig. 1a**). The use of microcantilevers with response time of ~0.5 µs and reading out the reflected laser beam at 0.05µs (high sampling rates up to 20 MSamples/s) allowed tracking the cantilever position while pulling at velocities up to ~30,000 µm/s (**Fig. 1**), almost an order of magnitude faster than previous HS-FS measurements and about 1000 times faster than conventional AFM FS measurements [11, 19, 29]. All atom steered molecular dynamics (MD) simulations precisely mimicked the experimental setup by using the fully solvated tetrameric structure of streptavidin (PDB 3RY2 [4]) and by pulling biotin using two springs in series, describing the PEG-linker and the cantilever, whose end was moved at constant velocity. The overall applied pulling velocities ranged from 0.05 µm/s to 30,000 µm/s in HS-FS experiments (**Fig. 1b**), and from 1,000 µm/s to $5 \cdot 10^{10}$ µm/s in SMD simulations (**Fig. 1c**), resulting in a combined range of loading rates from ~100 pN/s to ~10^{13} pN/s, covering eleven decades. Importantly, the wide experimental dynamic range up to such fast rates, together with recent simulation advances [30, 31], allowed direct overlap with *in silico* simulation loading rates over an entire decade between 10^8-10^9 pN/s (**Fig. 2 and SI**).

Experimental force curves showed a characteristic curvature of increasing force due to stretching of the flexible PEG linker (**Fig. 1**), signature of the specificity of the interaction [32] (cf. Supplemental Material). **Figure 2** shows the dynamic force spectrum obtained from both the most probable rupture forces at each loading rate (in pN/s) from experiments (circles) as well as the average of 10-20 simulations per loading rate (triangles). At overlapping loading rates, rupture forces from experiments and simulations agreed very well, thereby providing independent validation for the MD simulations. Up to ~10^6 pN/s (~10^3 µm/s pulling velocity), rupture forces increased linearly with the logarithm of the loading rate, indicating one single dominant barrier in this loading rate regime. At faster rates, steeper slopes are observed. This behavior has been interpreted before in terms of (a) additional, smaller transition barriers prior to the main barrier along the one-dimensional energy landscape, which become dominant at higher loading rates [10, 19], (b) force-induced shortening of the distance to the transition state [14, 33], and (c) a transition from a thermally activated to a so-called deterministic regime [15, 24, 34]. A fourth possible cause of a slope increase might be that the cantilever response time affects the force spectrum for pulling timescales shorter than the cantilever response time [35, 36]. Actually, previous experiments using devices with a dynamic response slower than HS-FS cantilevers (response time τ_c~50-500 µs, effective diffusion constant D_p~10^2-10^3 nm²/s, compared to τ_c~0.5 µs, D_p~10^5 nm²/s) have reported a marked slope increase at loading rates ~10^4 pN/s [10, 16, 19, 29], while our first slope increase occurred at ~10^6 pN/s. This suggests that HS-FS microcantilevers allow orders of magnitude faster loading rates before this possible effect may appear.

By virtue of the broad range of loading rates covered here, the combined dynamic force spectrum contains more information on the free energy landscape of unbinding than has been accessible before. Single barrier models did not describe the entire dynamic force spectrum satisfactorily, supporting the presence of a more complex energy landscape with multiple barriers [14, 15, 34, 36, 37] (**SI Fig. S5**). To avoid approximations inherent to analytic theories, we instead performed Brownian dynamics simulations with a more complex energy landscape with two barriers and varied the shape of this landscape (inset of **Fig. 2**, see also SI) to obtain the best fit to the dynamic force spectrum (blue line in **Fig. 2**). Importantly, this free energy landscape explains both experiment and simulation over the whole 11 orders of magnitude of loading rates. The energy landscape has an inner ~18 k_BT barrier at 0.11 nm, which determines the force spectrum slope at loading rates faster than 10^6 pN/s, and an outer ~21 k_BT barrier at 0.21 nm, which gives rise to the shallower slope at lower experimental rates (**Fig. 2** inset). The slope increase observed >10^{11} pN/s in the dynamic force spectrum could be explained by a transition from a

diffusion-dominated (Bell-Evans regime) to a deterministic regime [15, 34]. For SA-b, this critical loading rate ($\dot{F} >> F_c D x_\beta^{-2}$) ~$10^{11}$ pN/s (or ~10^{10} nm/s) is orders of magnitude faster than that observed in previous HS-FS experiments of titin unfolding (~10^7 pN/nm, ~10^6 nm/s) [24]. This was expected since the transition is supposed to emerge when the pulling rate is faster than the intrinsic time required for the complex to explore its energy landscape. This intrinsic time was (x_β^2/D) ~0.2 ms for titin I91, but much shorter (~0.3 ns) for SA/b, which is plausible given the smaller dimensions of the biotin molecule than the titin domain and was, thus, only accessible at simulation timescales.

The steered MD unbinding simulations (>300 in total) provided structural information on the loading rate dependent unbinding paths. **Figure 3A** shows the distribution of center of mass (COM) distances between the SA binding pocket and the biotin molecule from all MD trajectories. The peak at 0 nm represents the bound state followed by two consecutive minima at ~0.12 nm and ~0.25 nm. These values are close to the positions of the two barriers (~0.11 nm and ~0.21 nm) obtained from the BD fit of the force spectrum and suggest the COM distance as an appropriate reaction coordinate of unbinding. The simulations show that most of the H-bonds between biotin and the SA binding pocket remain intact until the biotin had moved ~0.1 nm towards the outside of the SA binding pocket. At the distance corresponding to the first barrier, the H-bonds between residues Asp128, Ser88, Asn23, Ala50 and Trp108 and the biotin, rather parallel to the pulling direction, rupture. Escape from the binding pocket occurs only at ~0.25 nm, where most of the remaining H-bonds between biotin and SA (mainly with residues Asn49, Tyr43 and Ser27) rupture. Notably, these H-bonds are nearly perpendicular to the unbinding direction (long axis of the binding pocket), which implies a shear force, and only simultaneous failure of all H-bonds lead to dissociation, with subsequent transient formation of a different H-bond network (**SI Fig. S7**). A similar mechanism has been observed before as key in providing stability against forced protein unfolding [38, 39].

One might assume that linear extrapolation of the force spectrum to zero force should yield a time scale similar to the spontaneous SA-b unbinding off-rate k_{off} ~10^{-6} s^{-1} obtained from bulk equilibrium experiments [7]. However, as in previous single molecule force experiments [10, 19] (see SI), **Figure 2** reveals a much faster rate of ~1 s^{-1}. Notably, also the predicted 22 $k_B T$, barrier height in the unbinding energy landscape is lower by ~18 $k_B T$, than both a Kramers estimate using an attempt frequency of 10^{12} s^{-1}, as well as the calorimetric SA-b binding free energy of ~40 $k_B T$ [7]. Whereas the end states of enforced and spontaneous unbinding are not the same and, hence, the respective (un)binding free energy differences are not expected to fully agree, such a large discrepancy is unexpected. Thus, to reconcile forced and equilibrium unbinding, a third barrier located further out on the unbinding pathway should be present, as was speculated before from indirect evidence [10, 21]. Such a barrier would, however, show up in a dynamic force spectrum at loading rates much lower than accessible to experiments (and certainly to simulations) and, therefore, remained so far unobserved. One would, therefore, expect to observe signatures of interaction between SA and biotin relatively farther out of the binding pocket, as structural determinants of this barrier.

Indeed, the MD simulations revealed such interactions and corresponding intermediate states. In particular, the COM distribution of distances between the SA binding pocket and the biotin molecule displays a pronounced peak after the second minimum followed by smaller peaks at distances up to 1.5 nm (**Fig. 3A and SI**). Detailed inspection of the individual MD trajectories showed as many as eight transient H-bonds (most importantly ASN49, GLU51 and TYR54) formed with biotin ~1 nm away from the binding pocket (**Fig. 3A**). Importantly, the force profiles from these trajectories displayed adhesive interactions after and at a lower value than the main force peak and, therefore, these states are not reflected in the dynamic force spectrum. In these events (**Fig. 3B**), the force applied to biotin displays a drop due to

the exit from the binding pocket and a subsequent intermediate force plateau with a final drop due to complete detachment. At the slowest MD velocities, this transient binding state lasted up to several hundred nanoseconds, such that it should also be detectable using HS-AFM microcantilevers with submicrosecond resolution.

To test this hypothesis, we analyzed in further detail the individual experimental force curves. Remarkably, we observed a similar signature in about 5% of the HS-FS unbinding events with a transient force plateau during the snap off of the cantilever (**Fig. 3C**). These transient, µs-long events were observed over the full range of experimental loading rates and provide an experimental signature of the transient outer states. Moreover, the distance from the force peak and the transient binding had an average value ~1 nm extending up to 3 nm (**Fig. 3D)**, similar to the distances seen in the MD trajectories (**Fig. 3A**). Therefore, the combination of HS-FS and MD simulations of SA/b forced unbinding provided first direct experimental evidence and a molecular description of an outer binding state that may be at the basis of the SA/b sturdiness.

The large number of experiments and simulations allowed us to characterize the average lifetime τ of these outer binding states. **Figure 3E** shows that τ ranges from 0.001 µs to 100 µs for forces F_i between 500 pN down to 20 pN (including MD and HS-FS data). Hence, excellent agreement between experiments and simulations is seen also in the time domain. The average lifetime decayed exponentially with force and can be modeled by a single barrier [14] of 12 $k_B T$ height with a rupture length of 0.16 nm and, notably, of ~16 µs-lifetime at zero force (**Fig. 3D**). This third barrier is located outwards adjacent to the two barriers shown in the inset of **Fig. 2** and adds a further step upwards to the energy landscape towards the fully unbound state, which further slows down biotin unbinding by several orders of magnitude, thereby reconciling it with the slow off-rate. The respective interactions between biotin and the outside of the binding pocket should favor rebinding events, in particular at low and zero forces. Although rare, back-and-forth fluctuations between intermediate states were actually observed in some of the MD trajectories (**Fig. 4**). Moreover, the corresponding pre-binding state would also provide an explanation of the high binding affinity of the SA-b complex as free biotin molecules may be transiently bound to solute exposed residues, before finally inserting into the binding pocket.

As shown in **Fig. 3D**, the experimental distance to the outer binding increased with the pulling velocity suggesting that shorter jumps occur more often at slow pulling. This suggests that, although effectively described by a single barrier, the outer barrier may involve not only one but several intermediate states, not directly resolved experimentally and with varying occupancies that depend on the pulling velocity. This notion is further supported by the various peaks observed in the COM distance outside of the binding pocket, which allowed characterizing the four most populated intermediate states (Int 1-4, **Fig. 4A**). Importantly, various unbinding paths were seen in the trajectories. The large number of atomistic simulations for each loading rate allowed us, finally, to study to what extent the observed unbinding pathways change with loading rate. Under high load, mainly two intermediate binding states (Int1 and Int2) are visited along the unbinding pathway. At lower loading rates, states Int3 and Int4, farther out, are also visited. Likely these, and even farther outside lying intermediates, provide a rugged funnel [40, 41, 42] for rebinding under equilibrium conditions.

Calculating and monitoring the average energy of the H-bonds between biotin and individual amino acids in the binding pocket from all MD trajectories as a function of the biotin position (**Fig. 4B and S7**) allowed us to extract structural snapshots of each intermediate state (**Fig. 4C**). Whereas the inner intermediate states showed strongest interactions between the ureido moiety of biotin and residues Ser27, Tyr43, and Asp128, respectively, at later stages of unbinding other bonds, largely

overlooked so far, become relevant, such as Arg84, Glu51 and Tyr54, at COM distances of up to 1.5 nm from the bound state. While streptavidin modifications of these three residues have reported lower biotin affinity [6, 43, 44], they have not been expected to be involved in biotin binding due to their large separation from the binding pocket and their little contribution to the bound state, underscoring the impact of features along the unbinding path on binding kinetics.

One could speculate that SA has evolved in tetrameric form because it allows for even larger binding affinity due to inter-monomeric stabilization, with the 7-8 loop providing the key inter-protomer interaction [5]. To test this idea, we repeated our steered MD simulations using monomeric streptavidin – which is difficult experimentally. As suggested before from high loading rate simulations on avidin-biotin unbinding [27], rupture forces of the monomer were systematically 10-20% lower than for the tetramer over the whole loading rate range (**Fig. S6**), thus further supporting this hypothesis. Closer structural analysis of the unbinding paths suggests that these reduced unbinding forces are due to (a) lacking inter-monomeric interactions (specifically to the 7-8 loop of the adjacent protomer [27]) and (b) an increased heterogeneity of unbinding paths, the larger entropy of which further reduces the unbinding barrier.

Strikingly, the unbinding rate dependent heterogeneity and occupancies of intermediate states is accompanied by a rate-dependent dynamics of the SA binding pocket. As an example, loop 3-4 switches between an open and a closed conformation during unbinding, depending on the distance between biotin and the binding pocket (**Fig S8**). This conformational dynamics is more pronounced for slower loading rates (**Fig S8**) and, therefore, should also occur in the AFM experiments as well as during spontaneous unbinding. This finding suggests that 'induced fit' motions do not only control the bound state, but also the energetics and kinetics of intermediate binding states.

The combination of HS-FS and MD simulations at overlapping loading rates allow us to obtain a dynamic, atomistic description of a receptor-ligand unbinding process. Characterizing enforced streptavidin/biotin unbinding over an unprecedentedly large range of loading rates enabled us to characterize large portions of the underlying energy landscape, which would not have been accessible by one of the two methods alone. Notably, it also allowed for a most direct comparison between AFM experiment and MD simulation. The excellent agreement of rupture forces – an observable that has never been used for force field parameterization – underscores the predictive power of atomistic simulations.

Our concerted approach revealed multiple unbinding pathways dependent on loading rate, with a detailed description of the pathway fluxes. In particular, outer intermediates were found that affect binding energetics and kinetics. Future combination of HS-FS and MD simulations will answer whether these proposed mechanisms found for SA/b are specific of this bond or, in our view more likely than not, a common feature of many receptor/ligand complexes and thus a general mechanism of regulating binding kinetics. If this were the case, the study of intermediates and their mechanism would be instrumental in improving the kinetics and specificity of drug-like compounds. Taken together, our results suggest that the lock-and-key paradigm may need revision in terms of many routes to the bound state as well as multiple, transient induced fits, alike a combination lock, where several intermediate positions have to be visited for release.
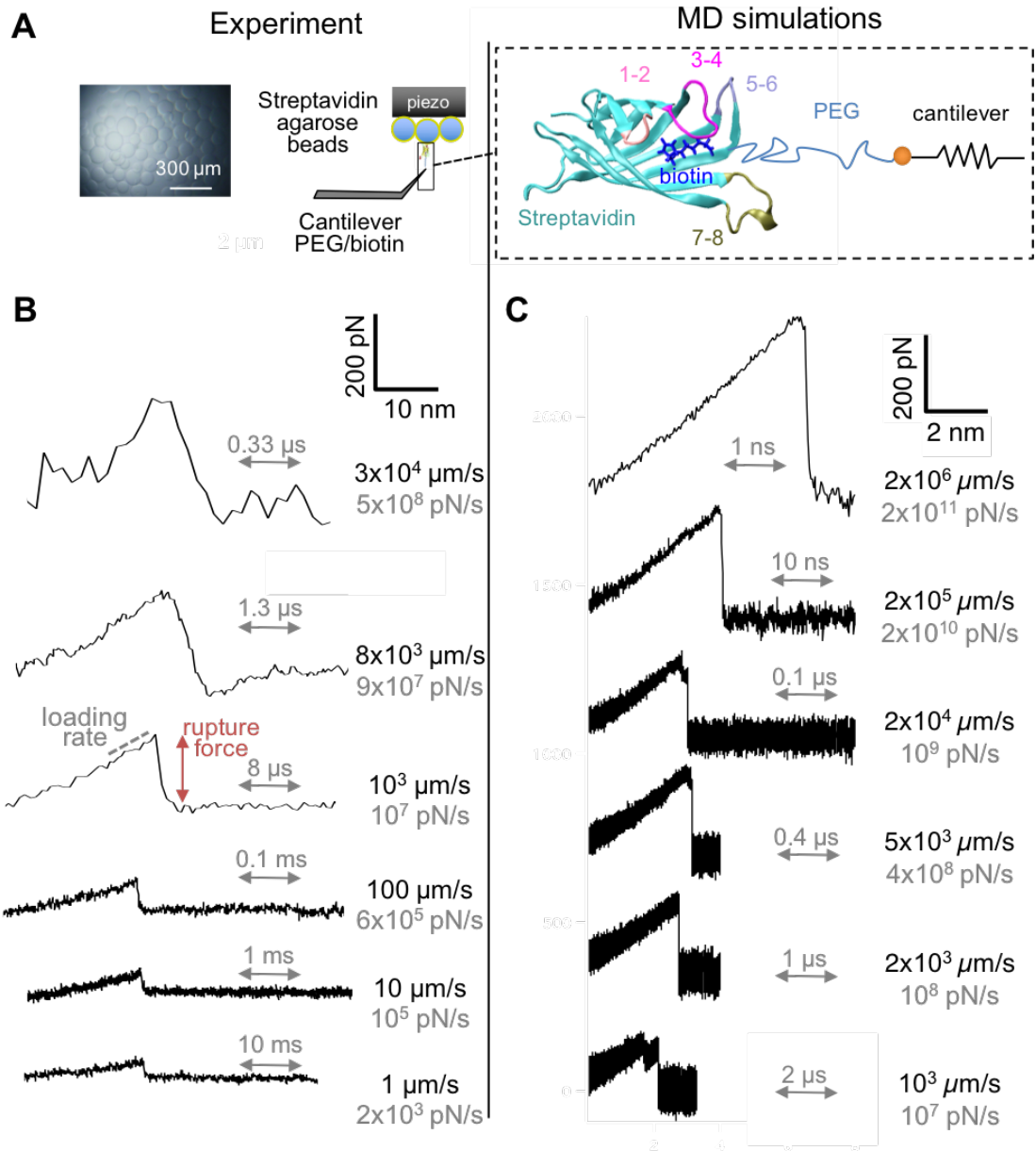
Fig. 1 High-speed and molecular dynamics force spectroscopy of streptavidin-biotin unbinding.

(A) High-speed force spectroscopy (HS-FS) setup. Streptavidin agarose beads (top left) were immobilized on the sample surface while biotin was covalently attached to the microcantilever (bottom left) through a polyethylene glycol (PEG) linker (contour length ~10 nm). Inset shows a streptavidin-biotin complex used in the MD simulations (blue, PDB 3RY2). **(B)** Experimental force-distance traces at velocities from 1 μm/s to 30,556 μm/s revealing bond rupture events using AC7 (top curve) and AC10 cantilevers (bottom curves). The stretching profile of the experimental curves was the results of stretching the PEG linker and deforming the agarose bead to which streptavidin was linked. **(C)** Force-extension traces from the MD simulations at retraction velocities from 2000 μm/s to 2×10^7 μm/s.
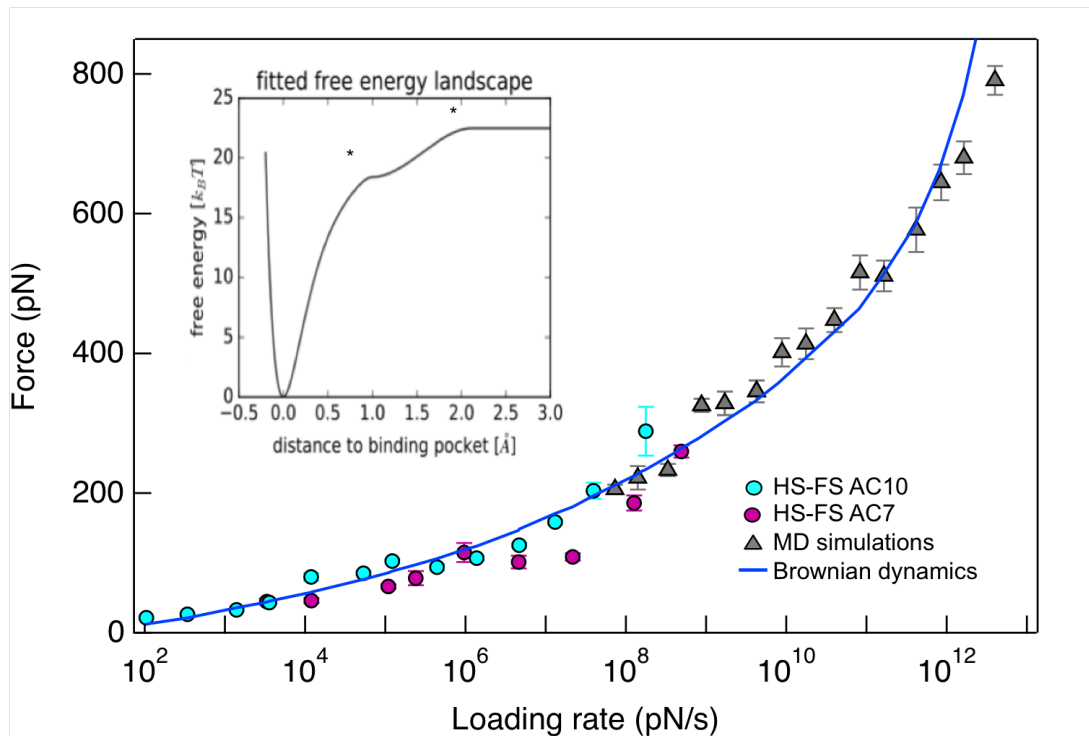
Fig. 2. Dynamic force spectrum of streptavidin/biotin unbinding. Most probable rupture forces from HS-FS experiments (●, using regular AC10 and fast AC7 cantilevers, cyan and magenta, respectively) and MD simulations (▲). The blue line represent the Brownian dynamics fit to the whole spectrum. The resulting energy landscape is shown in the inset and revealed two transition barriers (with parameters D = 4e9 nm^2/s, ΔG_1 = 18.4 k$_B$T, ΔG_2 = 21.1 k$_B$T, $x_{\beta1}$ = 0.11 nm, and $x_{\beta2}$ = 0.21 nm).
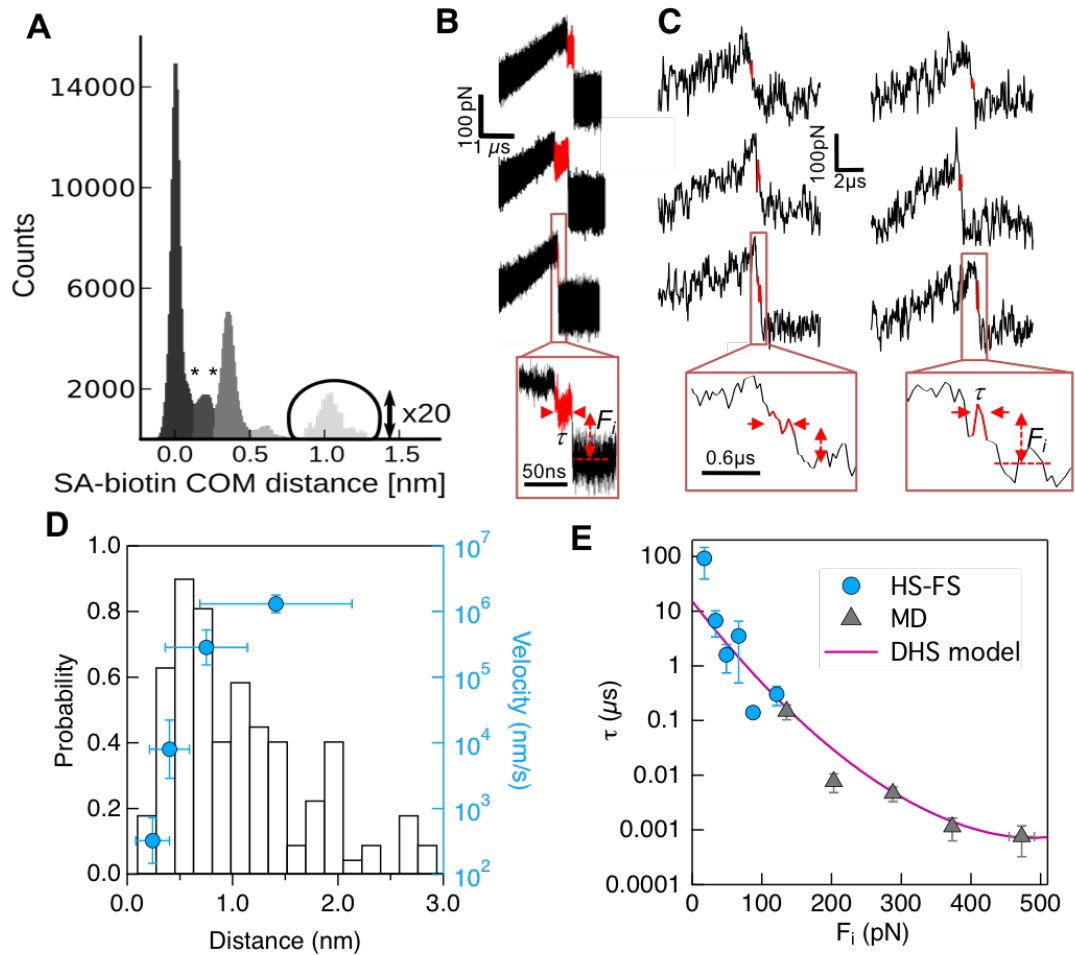
Fig. 3. Outer binding state. (A) Distribution of center of mass distances between streptavidin and biotin for all MD trajectories during unbinding. The first two minima coincide with the barrier position obtained from the Brownian dynamics simulations fit of the force spectrum in Fig. 2. (B) Examples of MD and (C) HS-FS force-time curves at 1000 μm/s. The lifetime and applied force of outer binding events was determined (red lines). (D) Distribution of experimental distance to outer binding (left axis) and pulling velocity dependence of the average distance (right axis) (E) Outer binding lifetime vs. applied force from HS-FS (●) and MD simulations (▲). The solid line shows the best fit to the force dependent lifetime DHS model [14] with parameters τ_0=16±7 μs, x$_\beta$=0.16±0.10 nm and ΔG=12±6 $k_B T$.
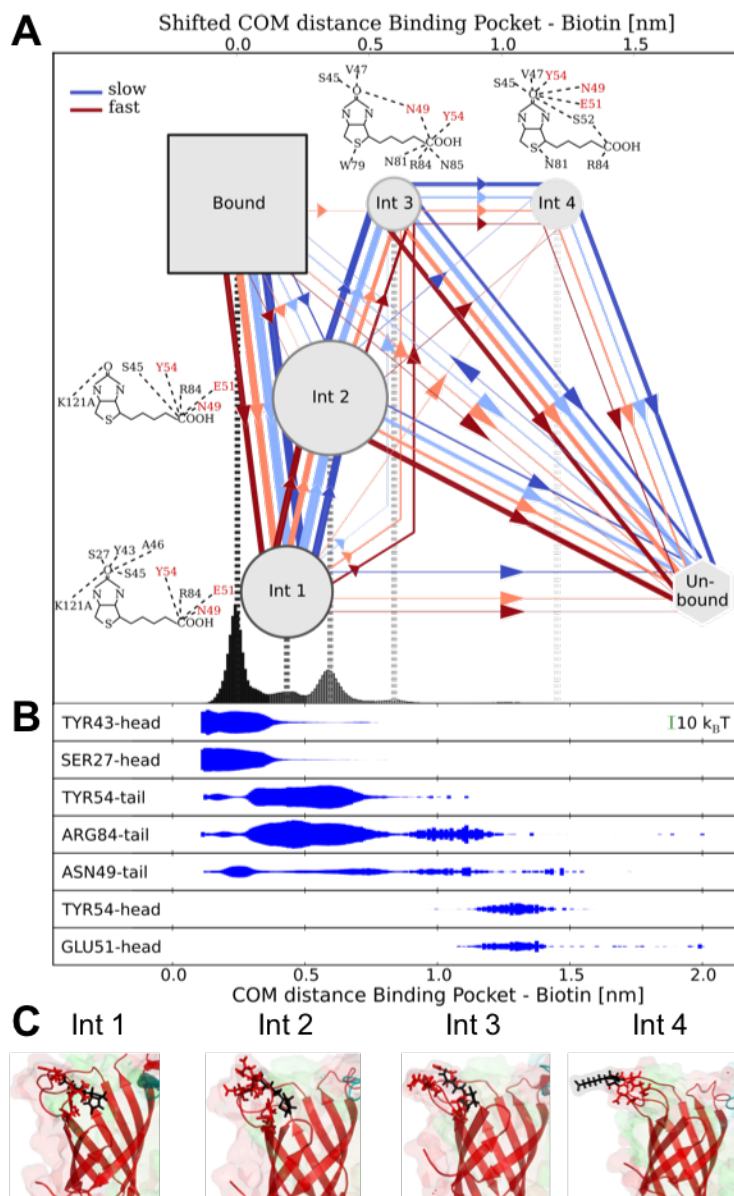
Fig. 4. Dynamic multiplicity of streptavidin-biotin unbinding pathways. (A) Bond and intermediate states with unbinding pathways observed during forced dissociation in MD trajectories. Line color reflects pulling velocity from slow to fast (blue to red) and thickness reflects passage probability. Biotin molecular representations show overlays of the hydrogen bonds with streptavidin residues for the four intermediate states. The energy of the H-bonds formed for the most important residues is shown below as a function of the COM distance. (B) Structural snapshots of the different intermediate states showing H-bonds between SA residues and biotin.

References

1.   Koshland DE. Application of a Theory of Enzyme Specificity to Protein
        Synthesis. *Proceedings of the National Academy of Sciences* 1958, **44**(2)**:**
        98-104.

2.   Fischer E. Einfluss der Configuration auf die Wirkung der Enzyme. *Berichte
        der deutschen chemischen Gesellschaft* 1894, **27**(3)**:** 2985-2993.

3.   Frederick KK, Marlow MS, Valentine KG, Wand AJ. Conformational entropy in
        molecular recognition by proteins: A first example from the calmodulin system.
        Nature 2007, **448**(7151)**:** 325-329.

4.   Le Trong I, Wang Z, Hyre DE, Lybrand TP, Stayton PS, Stenkamp RE.
        Streptavidin and its biotin complex at atomic resolution. *Acta
        Crystallographica Section D* 2011, **67**(9)**:** 813-821.

5.   Chilkoti A, Stayton PS. Molecular-Origins of the Slow Streptavidin-Biotin
        Dissociation Kinetics. *J Am Chem Soc* 1995, **117**(43)**:** 10622-10628.

6.   Laitinen OH, Hytonen VP, Nordlund HR, Kulomaa MS. Genetically engineered
        avidins and streptavidins. *Cell Mol Life Sci* 2006, **63**(24)**:** 2992-3017.

7.   Hyre DE, Le Trong I, Merritt EA, Eccleston JF, Green NM, Stenkamp RE*, et
        al.* Cooperative hydrogen bond interactions in the streptavidin-biotin system
        10.1110/ps.051970306. *Protein Sci* 2006, **15**(3)**:** 459-467.

8.   Koussa MA, Halvorsen K, Ward A, Wong WP. DNA nanoswitches: a
        quantitative platform for gel-based biomolecular interaction analysis. *Nat Meth*
        2015, **12**(2)**:** 123-126.

9.   Chivers CE, Crozat E, Chu C, Moy VT, Sherratt DJ, Howarth M. A streptavidin
        variant with slower biotin dissociation and increased mechanostability. *Nat
        Meth* 2010, **7**(5)**:** 391-393.

10.   Merkel R, Nassoy P, Leung A, Ritchie K, Evans E. Energy landscapes of
        receptor-ligand bonds explored with dynamic force spectroscopy. *Nature*
        1999, **397**(6714)**:** 50-53.

11.   Florin EL, Moy VT, Gaub HE. Adhesion Forces Between Individual Ligand-
        Receptor Pairs. *Science* 1994, **264**(5157)**:** 415-417.

12.   Lee GU, Kidwell DA, Colton RJ. Sensing Discrete Streptavidin Biotin
        Interactions with Atomic-Force Microscopy. *Langmuir* 1994, **10**(2)**:** 354-357.

13.   Evans E, Ritchie K. Dynamic strength of molecular adhesion bonds. *Biophys
        J* 1997, **72**(4)**:** 1541-1555.

14.   Dudko OK, Hummer G, Szabo A. Intrinsic rates and activation free energies
        from single-molecule pulling experiments. *Phys Rev Lett* 2006, **96**(10).

15.   Bullerjahn JT, Sturm S, Kroy K. Theory of rapid force spectroscopy. *Nat
        Commun* 2014, **5**.

16.   Teulon J-M, Delcuze Y, Odorico M, Chen S-wW, Parot P, Pellequer J-L. Single
        and multiple bonds in (strept)avidin–biotin interactions. *Journal of Molecular
        Recognition* 2011, **24**(3)**:** 490-502.

17.   Moy VT, Florin EL, Gaub HE. Intermolecular Forces and Energies Between Ligands and Receptors. *Science* 1994, **266**(5183)**:** 257-259.

18.   Sedlak SM, Bauer MS, Kluger C, Schendel LC, Milles LF, Pippig DA*, et al.* Monodisperse measurement of the biotin-streptavidin interaction strength in a well-defined pulling geometry. *PLOS ONE* 2017, **12**(12)**:** e0188722.

19.   Rico F, Moy VT. Energy landscape roughness of the streptavidin-biotin interaction. *J Mol Recognit* 2007, **20**(6)**:** 495-501.

20.   Jeney S, Mor F, Koszali R, Forró L, Moy VT. Monitoring ligand–receptor interactions by photonic force microscopy. *Nanotechnology* 2010, **21**(25)**:** 255102.

21.   Pincet F, Husson J. The solution to the streptavidin-biotin paradox: The influence of history on the strength of single molecular bonds. *Biophys J* 2005, **89**(6)**:** 4374-4381.

22.   Neupane K, Foster DA, Dee DR, Yu H, Wang F, Woodside MT. Direct observation of transition paths during the folding of proteins and nucleic acids. *Science* 2016, **352**(6282)**:** 239-242.

23.   Yu H, Siewny MGW, Edwards DT, Sanders AW, Perkins TT. Hidden dynamics in the unfolding of individual bacteriorhodopsin proteins. *Science* 2017, **355**(6328)**:** 945-950.

24.   Rico F, Gonzalez L, Casuso I, Puig-Vidal M, Scheuring S. High-Speed Force Spectroscopy Unfolds Titin at the Velocity of Molecular Dynamics Simulations. *Science* 2013, **342**(6159)**:** 741-743.

25.   Takahashi H, Rico F, Chipot C, Scheuring S. α-Helix Unwinding as Force Buffer in Spectrins. *ACS Nano* 2018, **12**(3)**:** 2719-2727.

26.   Grubmuller H, Heymann B, Tavan P. Ligand binding: Molecular mechanics calculation of the streptavidin biotin rupture force. *Science* 1996, **271**(5251)**:** 997-999.

27.   Izrailev S, Stepaniants S, Balsera M, Oono Y, Schulten K. Molecular dynamics study of unbinding of the avidin-biotin complex. *Biophysical Journal* 1997, **72**(4)**:** 1568-1581.

28.   Walton EB, Lee S, Van Vliet KJ. Extending Bell's model: How force transducer stiffness alters measured unbinding forces and kinetics of molecular complexes. *Biophysical Journal* 2008, **94**(7)**:** 2621-2630.

29.   Yuan C, Chen A, Kolb P, Moy VT. Energy landscape of streptavidin-biotin complexes measured by atomic force microscopy. *Biochemistry (Mosc)* 2000, **39**(33)**:** 10219-10223.

30.   Abraham MJ, Murtola T, Schulz R, Páll S, Smith JC, Hess B*, et al.* GROMACS: High performance molecular simulations through multi-level parallelism from laptops to supercomputers. *SoftwareX* 2015, **1:** 19-25.

31.   Kutzner C, Páll S, Fechner M, Esztermann A, de Groot BL, Grubmüller H. Best bang for your buck: GPU nodes for GROMACS biomolecular simulations. *J Comput Chem* 2015, **36**(26)**:** 1990-2008.

32.   Hinterdorfer P, Baumgartner W, Gruber HJ, Schilcher K, Schindler H. Detection and localization of individual antibody-antigen recognition events by atomic force microscopy. *Proc Natl Acad Sci U S A* 1996, **93**(8)**:** 3477-3481.

33.   Heymann B, Grubmüller H. Dynamic force spectroscopy of molecular adhesion bonds. *Physical Review Letters* 2000, **84**(26)**:** 6126.

34.   Hummer G, Szabo A. Kinetics from nonequilibrium single-molecule pulling experiments. *Biophys J* 2003, **85**(1)**:** 5-15.

35.   Makarov DE. Communication: Does force spectroscopy of biomolecules probe their intrinsic dynamic properties? *The Journal of Chemical Physics* 2014, **141**(24)**:** 241103.

36.   Cossio P, Hummer G, Szabo A. Kinetic Ductility and Force-Spike Resistance of Proteins from Single-Molecule Force Spectroscopy. *Biophysical Journal* 2016, **111**(4)**:** 832-840.

37.   Friddle RW, Noy A, De Yoreo JJ. Interpreting the widespread nonlinear force spectra of intermolecular bonds. *Proceedings of the National Academy of Sciences* 2012, **109**(34)**:** 13573-13578.

38.   Lu H, Schulten K. The Key Event in Force-Induced Unfolding of Titin s Immunoglobulin Domains. *Biophysical Journal* 2000, **79**(1)**:** 51-65.

39.   Grater F, Shen J, Jiang H, Gautel M, Grubmuller H. Mechanically induced titin kinase activation studied by force-probe molecular dynamics simulations. *Biophys J* 2005, **88**(2)**:** 790-804.

40.   Wolynes PG. Folding funnels and energy landscapes of larger proteins within the capillarity approximation. *Proceedings of the National Academy of Sciences* 1997, **94**(12)**:** 6170-6175.

41.   Voß B, Seifert R, Kaupp UB, Grubmüller H. A quantitative model for camp binding to the binding domain of mlok1. *Biophys J* 2016, **111**(8)**:** 1668-1678.

42.   Wang J, Verkhivker GM. Energy landscape theory, funnels, specificity, and optimal criterion of biomolecular binding. *Phys Rev Lett* 2003, **90**(18)**:** 188101.

43.   Hohsaka T, Muranaka N, Komiyama C, Matsui K, Takaura S, Abe R*, et al.* Position-specific incorporation of dansylated non-natural amino acids into streptavidin by using a four-base codon. *FEBS Letters* 2004, **560**(1)**:** 173-177.

44.   Murakami H, Hohsaka T, Ashizuka Y, Hashimoto K, Sisido M. Site-Directed Incorporation of Fluorescent Nonnatural Amino Acids into Streptavidin for Highly Sensitive Detection of Biotin. *Biomacromolecules* 2000, **1**(1)**:** 118-125.

Heterogeneous and rate-dependent streptavidin-biotin unbinding revealed by high-speed force spectroscopy and molecular dynamics simulations

Felix Rico[‡][*], Andreas Russek[‡], Laura González, Helmut Grubmüller[*], and Simon Scheuring[*]

[*] Corresponding authors
[‡] Equal contribution

correspondence to: felix.rico@inserm.fr, sis2019@med.cornell.edu, hgrubmu@gwdg.de

This supplementary information file includes:

Materials and Methods
Supplementary text
Figures S1 – S8
References (45-66)

Materials and Methods

HS-AFM tips and sample preparation

Streptavidin coated 4% agarose beads (Sigma) were immobilized on the sample surface by embedding them in a thin agarose layer. Biotin was covalently attached to the cantilever through a polyethylene glycol (PEG) linker (stretched length ~10 nm, Fig. 1A). Briefly, HS-AFM (AC10DS and AC7) cantilevers (Olympus, Japan) were rinsed with acetone for 10 min, plasma cleaned for 5 min in O_2 and immersed in a solution of 10-20 mg/ml silane-PEG-biotin (1 kDa, Nanocs Inc, NY) in ethanol/water (95/5). After 2 h incubation, cantilevers were rinsed with ultrapure water and stored at 4°C until use.

HS-FS measurements

HS-FS measurements were carried out on an HS-AFM (RIBM, Japan) featuring a high-speed acquisition board system (PXI, National Instruments, Texas, USA) to control the z−movement and acquire force curves at sampling rates up to 20 MS/s. Two types of cantilevers with submicrosecond time response and small viscous damping were used: AC10 cantilevers with 600 kHz resonance frequency in liquid, 0.1 N/m spring constant, quality factor of 0.9, and 0.09 pN μm^{-1} s^{-1} viscous coefficient; and shorter AC7 cantilevers, with 1.3 MHz resonance frequency in liquid, 0.6 N/m spring constant, quality factor of 0.6, and 0.05 pN μm^{-1} s^{-1} viscous coefficient. The spring constant of the cantilevers was determined in air using the Sader method [45]. The optical lever sensitivity was then determined in liquid from the thermal spectrum and the known spring constant [46] [47]. Short HS-AFM cantilevers were placed on the cantilever holder immersed in the fluid cell with PBS (phosphate-buffered saline) buffer and placed on the HS-AFM. The streptavidin agarose functionalized sample-stage was then mounted onto the fluid cell. Force curves were collected approaching the sample at a constant speed of 10 μm/s and indenting the streptavidin agarose with the biotinylated tip for 0.5 s at a constant force of <500 pN. The sample was then retracted at varying retraction velocities from 0.010 μm/s to 30,000 μm/s. Free biotin was titrated into the fluid cell to achieve a lower binding frequency of ~5% favoring single-bond interactions, assuring that most of the events (>95%) reported single bond ruptures [48, 49]. The reduction in binding frequency after adding free biotin further confirmed the specificity of the interaction. Representative examples of retraction force curves are shown in figure 1B. The sampling rate was set between 2 MS/s and 20 MS/s depending on the retraction speed of the experiment.

Data processing

Force curves presenting rupture events were analyzed using semi-automated software (Matlab, Mathworks) to measure the rupture forces, rupture lengths and effective spring constant (Fig. 1B). Loading rates were determined from the slope before rupture (2-3 nm) of each force versus time trace. Rupture forces were pooled by loading rate and the corresponding histograms generated (Supplementary Figs. S1 and S2). Most probable rupture forces and standard deviations of rupture forces at each loading rate were calculated from Gaussian fits (Supplementary Figs. S1 and S2). When two peaks were clearly distinguishable in the force histograms, distributions were fitted using a bimodal function imposing the center of the second peak to be 2 times that of the first peak. Thus, the first center peak value was used as the average rupture force (Supplementary Figs. S1 and S2).

Viscous drag correction

Viscous drag coefficients were calculated for each cantilever type from retraction curves by measuring the drag force exerted on the cantilever at various velocities near the substrate (<200 nm) divided by the retraction velocity [50, 51]. The cantilever coefficients on agarose beads were 0.09 pN/(µm/s) and 0.05 pN/(µm/s) for AC10 and AC7 cantilevers, respectively. The viscous drag was corrected by multiplying the viscous drag coefficient by the relative tip velocity. This correction was only significant (~8% force correction) at the highest velocities achieved with each cantilever type.

Molecular dynamics simulations

Force probe molecular dynamics simulations were carried out using the Amber99sb [52] force field together with TIP3P [53] water model and virtual interaction sites [54]. The electrostatic interaction was calculated with particle-mesh Ewald [Darden et al., 1993] with a real space cut-off of 1 nm, a grid spacing of 0.12 nm and cubic interpolation. The same cut-off length was used for the Van-der-Waals interaction. All atom bonds were constraint using LINCS algorithm [55]. All simulations were performed at a constant number of particles and a constant temperature coupled to a heat bath at 300 K using the velocity rescaling method [56] and a coupling constant of 0.2 ps. We used the Verlet algorithm [57] with a time step of 4 fs to integrate the equation of motion. In the experimental setup, the cantilever, here described by a harmonic potential with a spring constant k_{pull} = 100 pN/nm, was attached to Biotin via a PEG-linker. The harmonic potential was moved away from the binding pocket at 12 different velocities, ranging from 0.001 m/s up to 50 m/s. In the simulations the linker was described by a worm like chain potential with a persistence length l_p = 1.4 nm and a contour length l_c= 10 nm (Fig. 1 sim setup). All simulations were performed at a sodium chloride concentration of 150 mM. The starting structure for the simulations was based on the tetramer PDB-ID 3RY2 [58]. In case of the tetramer, only one Biotin was pulled out of the binding pocket to ensure single unbinding events.

Center of Mass distributions

To calculate the distributions of the center of mass (COM) distance of each MD trajectory, we calculated the distance between the center of mass of the binding pocket forming residues (L25, S27, Y43, S45, V47, G48, A50, W79, R84, A86, S88, T90, W92, W108, L110, D128) and the center of mass of biotin. This was done starting shortly before rupture and ending when the distance between biotin and the binding pocket was larger 4 nm.

As we do not see any binding patterns further away than 2 nm we reduced the plotted histograms to a maximal distance of 2 nm. The COM distances were then binned into 200 equally spaced bins and normalized by the total amount of data points.

Intermediate states and transition plots

To determine the intermediate states, we split the COM distance distributions according to the dominant peaks, such that each peak represents a different intermediate state. We then calculated the transition rates by counting the transitions from state s_i to state s_j and subtracted the amount of back-transitions (s_j to s_i) for each combination, resulting in a net flux of either -1, 0 or 1. Finally each rate was averaged for each velocity.

The probabilities for being in an intermediate state where calculated by counting the total time that an intermediate state is visited normalized by the total time spent in all

intermediate states. The time spent in the ground state and the unbound state were not taken into account to provide comparability, as the time spent in either of them is arbitrary and depends only on the chosen starting- and endpoint of the rupture event.

Supplementary Text

<u>Previous single molecule force spectroscopy of the streptavidin/biotin complex</u>

The complex formed by streptavidin (SA) and the small molecule biotin (b, vitamin H) is one of the strongest non-covalent bonds known in nature. Monomeric streptavidin forms the biotin-binding pocket with an eight-stranded, antiparallel beta-barrel capped by loop 3-4. In the native, tetrameric SA, loop 7-8 from an adjacent monomer contributes to closing the binding pocket and was shown important to preserve the binding properties of the complex [59]. Biotin binds by forming an intricate network of hydrogen bonds with polar residues of both the beta-barrel and loop 3-4 [58, 60]. Due to its high affinity ($K_D \sim 10^{-13}$ M) and long lifetime ($k_{off} \sim 10^{-6}$ s^{-1}, ~ 0.1 day^{-1}) as measured from bulk, equilibrium measurements [61, 62, 63, 64], the SA-b complex is extensively used in molecular biology for protein labeling and purification. SA-b is also widely used in biotechnology and single molecule measurements to immobilize proteins, DNA and RNA molecules on surfaces as it supports large pulling forces [65]. The forced disruption of the streptavidin-biotin complex by atomic force microscopy (AFM) and other techniques established the basis of single molecule biomechanics [63, 64, 66, 67, 68, 69, 70, 71, 72, 73, 74, 75, 76, 77, 78, 79]. However, single molecule experiments on the SA-b complex often estimated the intrinsic unbinding rate to be orders of magnitude faster than off-rates measured from bulk-equilibrium experiments ($\sim 10^{-6}$ s^{-1}), and data diverge, although this divergence seems to disappear if low binding frequency (highe probability of probing single bonds) is assured [49]. Nevertheless, also bulk experiments have reported dissimilar intrinsic unbinding rates [61, 62]. All atom steered molecular dynamics simulations (SMDS) of the forced unbinding of SA-b were pioneer in the field and have provided mechanistic descriptions of the unbinding process [80, 81]. However, due to limited computational power for SMDS, the number of studies assessing the dynamic nature of the bond are still rare and were performed either on monomeric SA or at pulling velocities several orders of magnitude faster than experiments, precluding direct comparison [70, 71, 80, 81, 82, 83, 84, 85]. Thus, knowledge of the dynamic nature of the SA-b bond and its (un)binding process is still limited, i.e. it is still unknown how this non-covalent bond outlives days.

<u>Bimodal distributions</u>

Bimodal distributions in force histograms have been attributed to simultaneous double bond rupture events and cooperative effects at the high forces reached at fast loading rates [68, 74, 77, 86]. Using cantilevers with shorter time response minimized the occurrence of bimodal distributions (**SI**), probably because they allowed easier discrimination between curves with single and double rupture events even at the highest velocities.

Fig. S1
Rupture force distributions using AC10 cantilevers at different loading rates indicating the number of analyzed events per plot. Solid lines are best fits to a single (red) and double (green) gaussian distributions. When a double distribution was used, the most probable force was determined from the first peak.
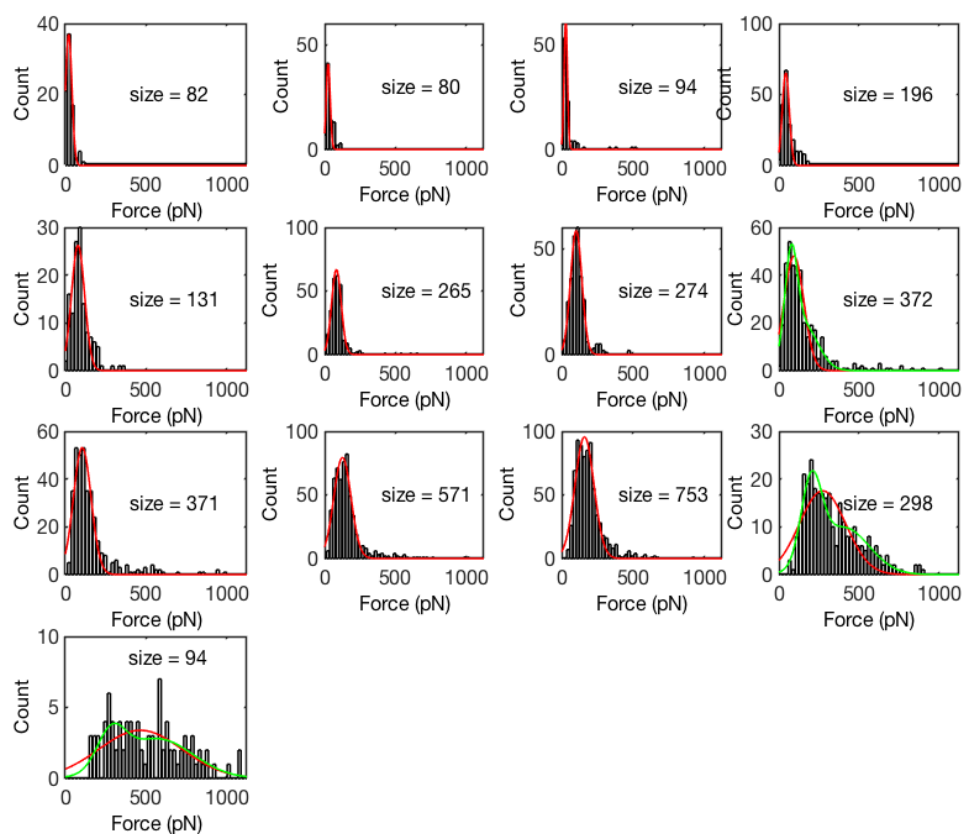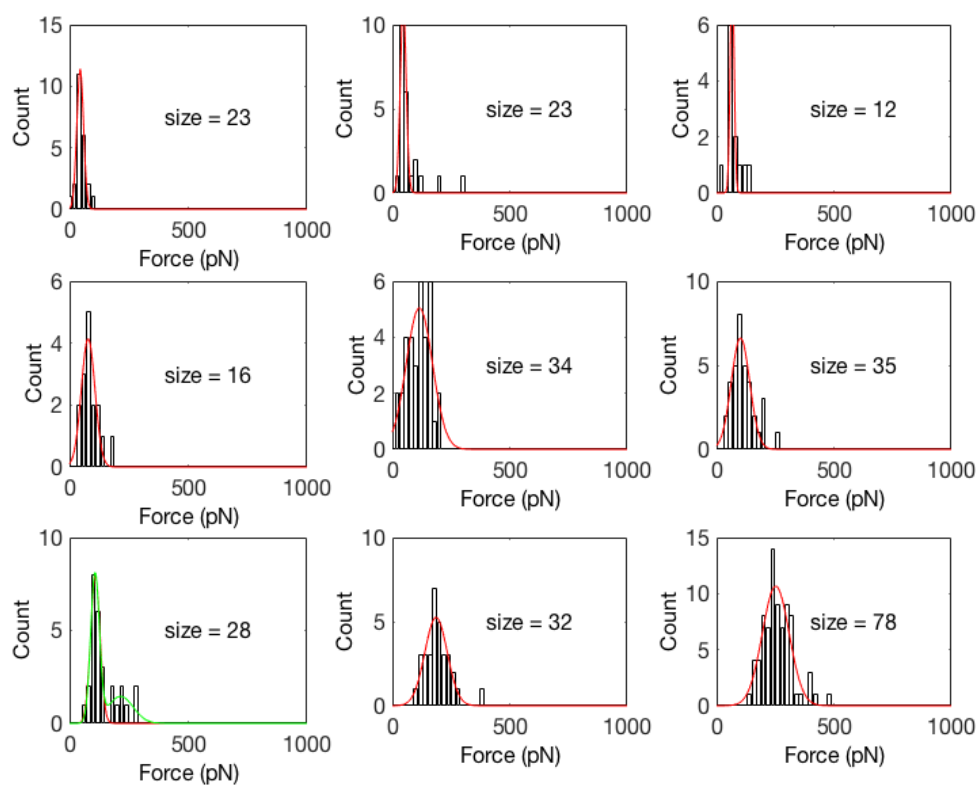
Fig. S2

Rupture force distributions using AC7 cantilevers at different loading rates indicating the number of analyzed events per plot. Solid lines are best fits to a single (red) and double (green) gaussian distributions. When a double distribution was used, the most probable force was determined from the first peak.

Fig. S3

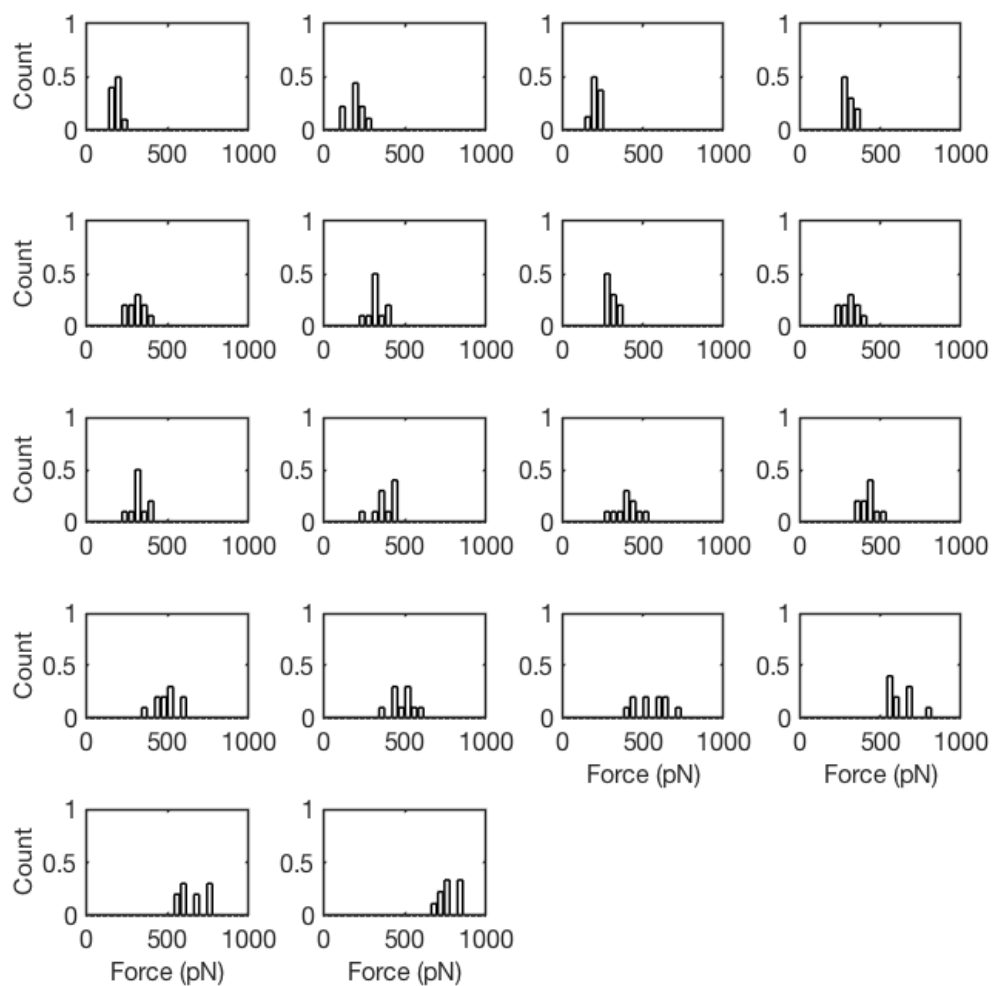Rupture force distributions from tetrameric SA/b MD simulation trajectories at different retraction velocities.

Fig. S4.
Rupture force distributions from monomeric SA/b MD simulation trajectories at different retraction velocities.
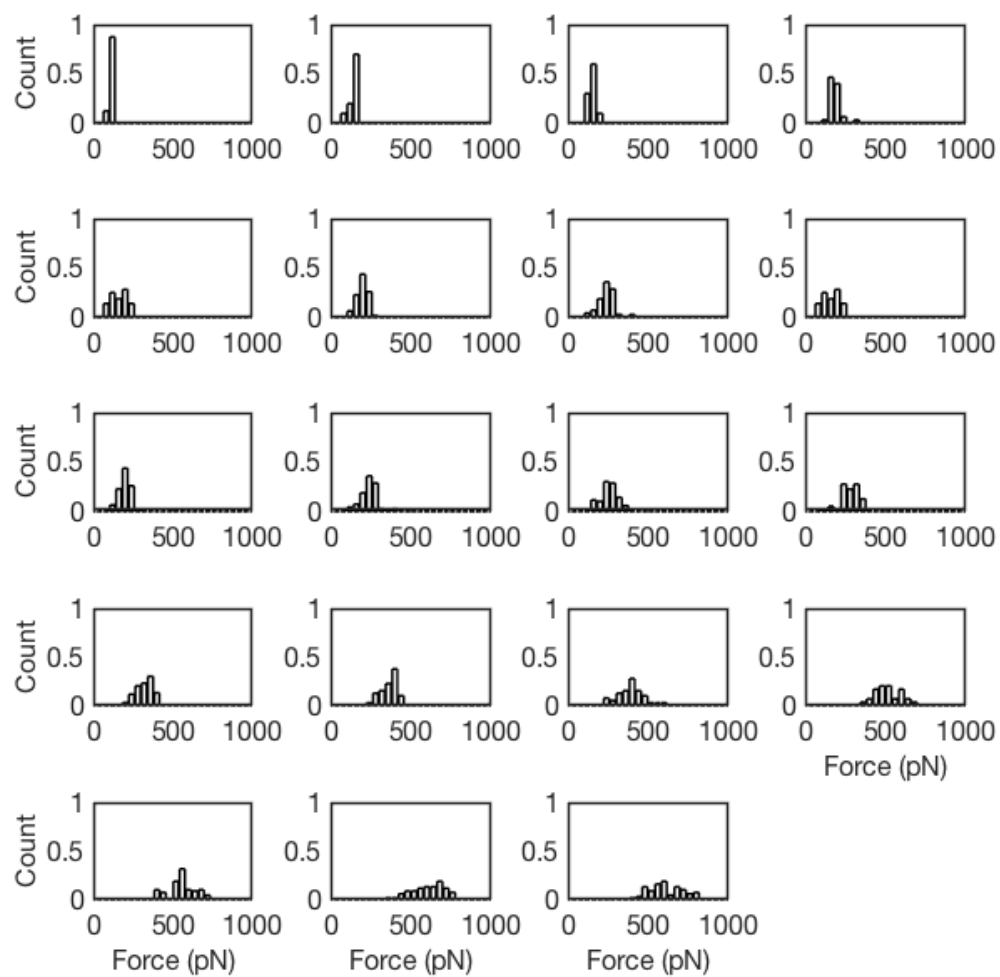
Fig. S5

Experimental and MD simulations dynamic force spectra of the SA/b interaction. Solid lines are the best fits of the BSK [87], FNdY [88], DHS [75] and CHS [89] models to the combined dynamic force spectrum.

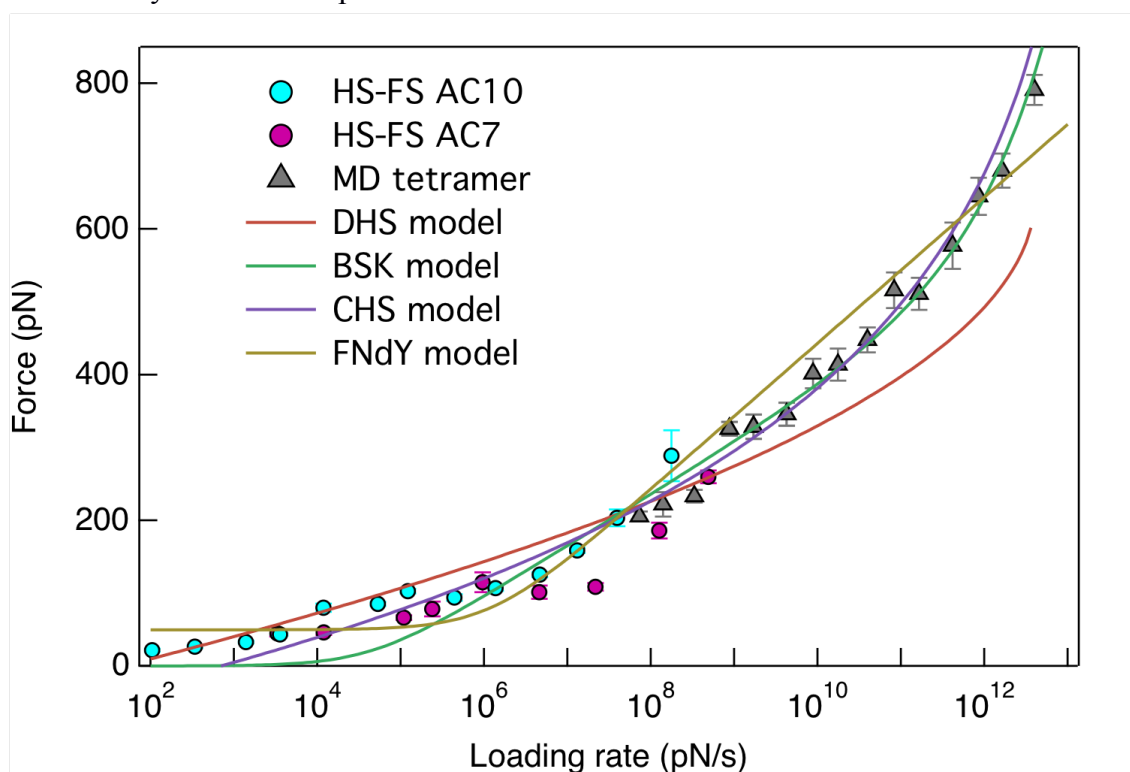**Fig. S6**

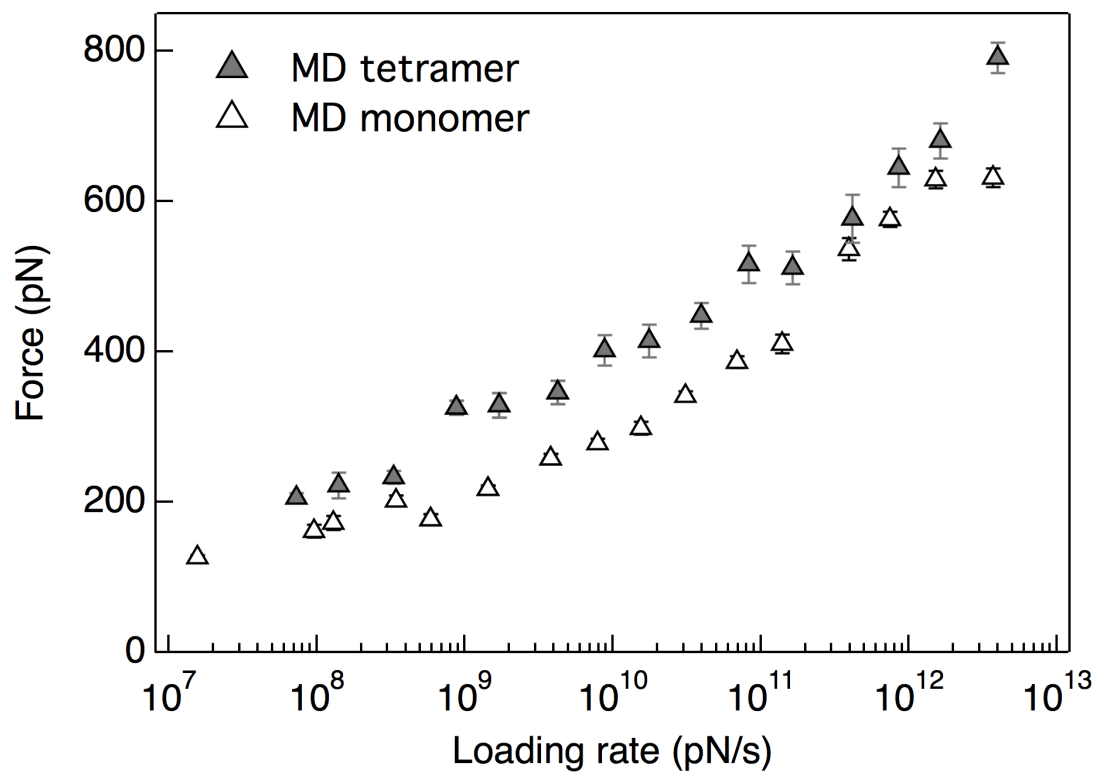Comparison between monomeric and tetrameric streptavidin-biotin MD force spectra.
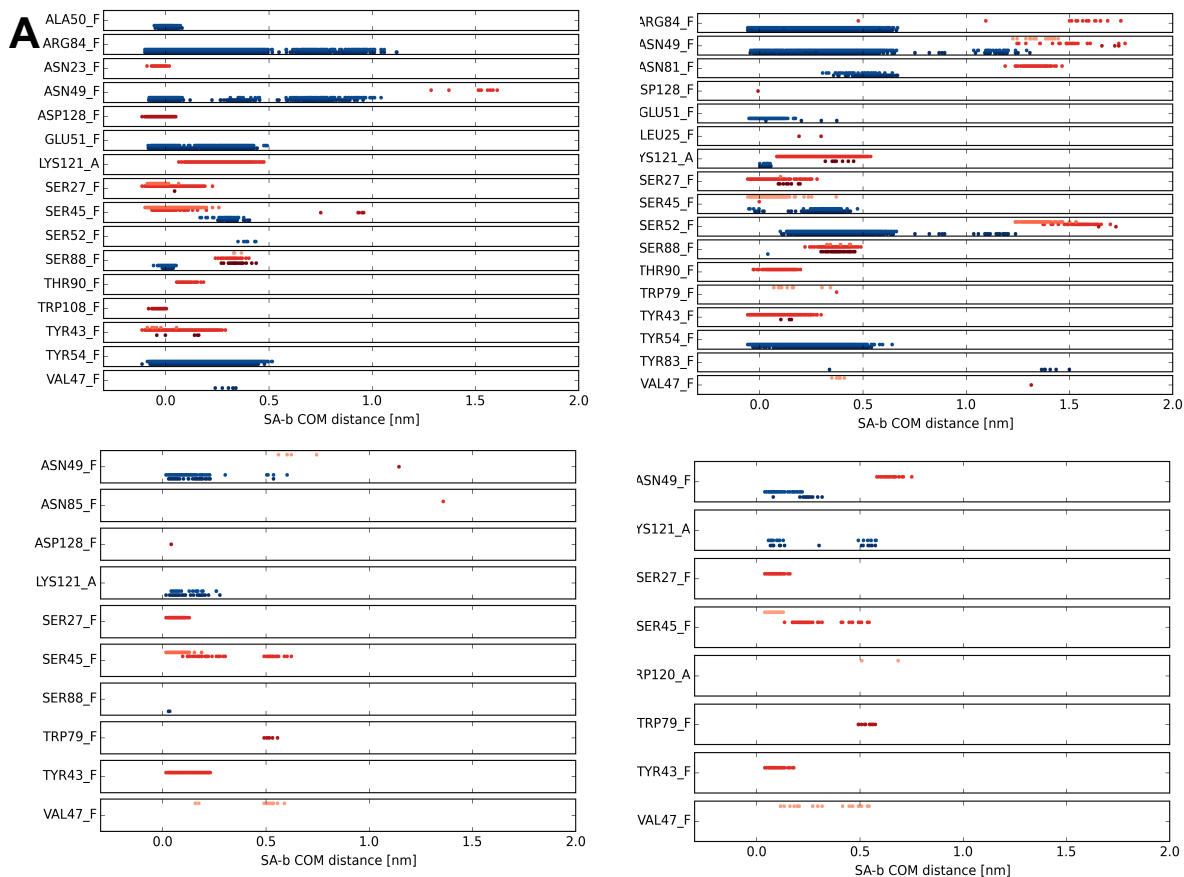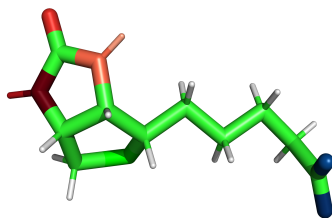
Fig. S7

Examples of simultaneous bond rupture of H-bonds with subsequent building of new binding patterns at different velocity regimes. Each subplot shows the existence of H-bonds between the named amino acids and biotin. F stands for the SA monomer out of which biotin is pulled and A for an adjacent SA monomer. The color of the dots refers to the interaction partner of biotin. Red colors stand for interactions with the head group of biotin as shown in B. The blue dots are H-bonds formed with the tail of
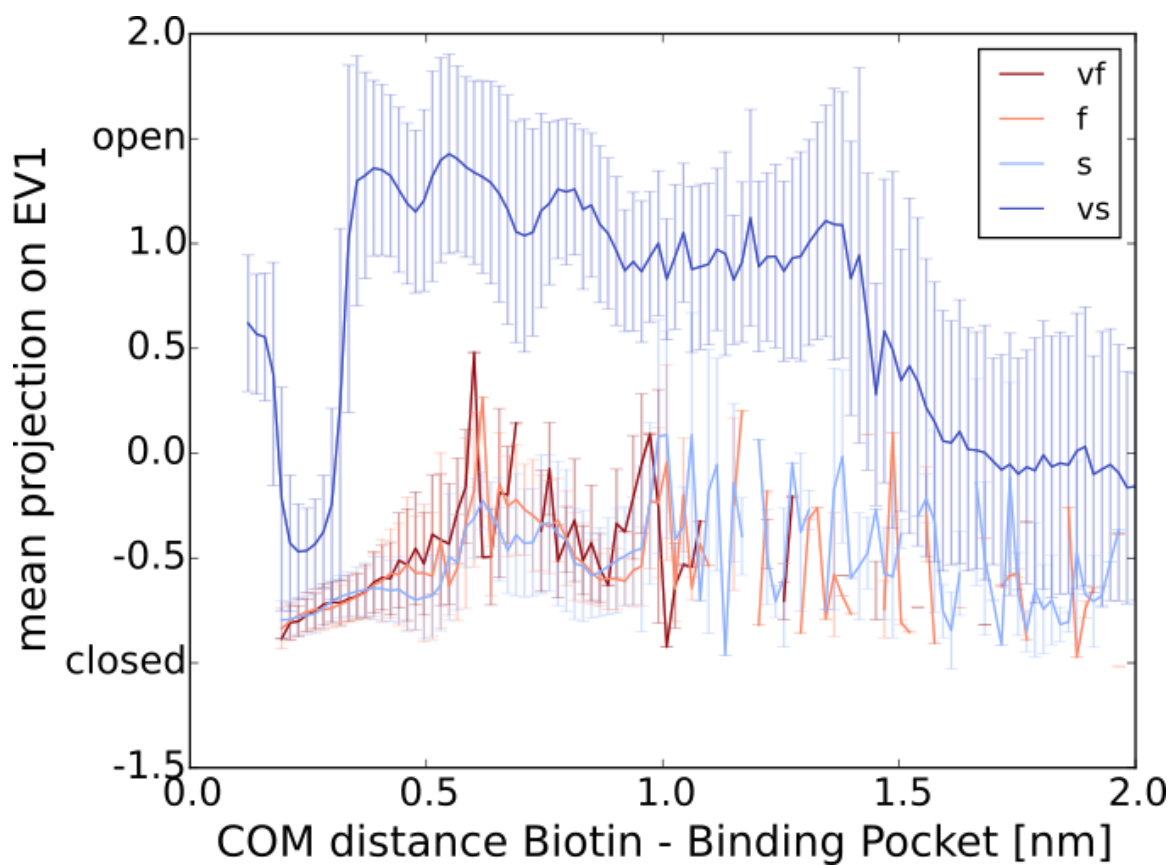

biotin

Fig. S8

Projection of all trajectories onto the first eigenvector of a PCA of the loop3-4 motion plotted over the COM distance between the binding pocket and biotin. Different colors denote different pulling velocity regimes ranging from fast (red) to slow (blue).

References

45.   Sader JE, Borgani R, Gibson CT, Haviland DB, Higgins MJ, Kilpatrick JI, *et al.* A virtual instrument to standardise the calibration of atomic force microscope cantilevers. *Review of Scientific Instruments* 2016, **87**(9)**:** 093711.

46.   Rico F, Gonzalez L, Casuso I, Puig-Vidal M, Scheuring S. High-Speed Force Spectroscopy Unfolds Titin at the Velocity of Molecular Dynamics Simulations. *Science* 2013, **342**(6159)**:** 741-743.

47.   Sumbul F, Marchesi A, Takahashi H, Scheuring S, Rico F. High-Speed Force Spectroscopy for Single Protein Unfolding. In: Lyubchenko YL (ed). *Nanoscale Imaging: Methods and Protocols*. Springer New York: New York, NY, 2018, pp 243-264.

48.   Tees DFJ, Waugh RE, Hammer DA. A microcantilever device to assess the effect of force on the lifetime of selectin-carbohydrate bonds. *Biophys J* 2001, **80**(2)**:** 668-682.

49.   Johnson KC, Thomas WE. How Do We Know when Single-Molecule Force Spectroscopy Really Tests Single Bonds? *Biophysical journal* 2018, **114**(9)**:** 2032-2039.

50.   Janovjak HJ, Struckmeier J, Muller DJ. Hydrodynamic effects in fast AFM single-molecule force measurements. *European Biophysics Journal with Biophysics Letters* 2005, **34**(1)**:** 91-96.

51.   Alcaraz J, Buscemi L, Puig-de-Morales M, Colchero J, Baro A, Navajas D. Correction of microrheological measurements of soft samples with atomic force microscopy for the hydrodynamic drag on the cantilever. *Langmuir* 2002, **18**(3)**:** 716-721.

52.   Hornak V, Abel R, Okur A, Strockbine B, Roitberg A, Simmerling C. Comparison of multiple Amber force fields and development of improved protein backbone parameters. *Proteins: Structure, Function, and Bioinformatics* 2006, **65**(3)**:** 712--725.

53.   Jorgensen WL, Chandrasekhar J, Madura JD, Impey RW, Klein ML. Comparison of simple potential functions for simulating liquid water. *The Journal of chemical physics* 1983, **79**(2)**:** 926--935.

54.   Feenstra KA, Hess B, Berendsen HJC. Improving efficiency of large time-scale molecular dynamics simulations of hydrogen-rich systems. *Journal of Computational Chemistry* 1999, **20**(8)**:** 786--798.

55. Hess B, Bekker H, Berendsen HJC, Fraaije JGEM. LINCS: a linear constraint solver for molecular simulations. *Journal of computational chemistry* 1997, **18**(12)**:** 1463--1472.

56. Bussi G, Donadio D, Parrinello M. Canonical sampling through velocity rescaling. *The Journal of chemical physics* 2007, **126**(1)**:** 014101.

57. Verlet L. Computer" experiments" on classical fluids. I. Thermodynamical properties of Lennard-Jones molecules. *Physical review* 1967, **159**(1)**:** 98.

58. Le Trong I, Wang Z, Hyre DE, Lybrand TP, Stayton PS, Stenkamp RE. Streptavidin and its biotin complex at atomic resolution. *Acta Crystallographica Section D* 2011, **67**(9)**:** 813-821.

59. Freitag S, Le Trong I, Klumb L, Stayton P, Stenkamp R. Structural studies of the streptavidin binding loop. *Protein science: a publication of the Protein Society* 1997, **6**(6)**:** 1157-1166.

60. Chilkoti A, Stayton PS. Molecular-Origins of the Slow Streptavidin-Biotin Dissociation Kinetics. *J Am Chem Soc* 1995, **117**(43)**:** 10622-10628.

61. Laitinen OH, Hytonen VP, Nordlund HR, Kulomaa MS. Genetically engineered avidins and streptavidins. *Cell Mol Life Sci* 2006, **63**(24)**:** 2992-3017.

62. Hyre DE, Le Trong I, Merritt EA, Eccleston JF, Green NM, Stenkamp RE*, et al.* Cooperative hydrogen bond interactions in the streptavidin-biotin system 10.1110/ps.051970306. *Protein Sci* 2006, **15**(3)**:** 459-467.

63. Koussa MA, Halvorsen K, Ward A, Wong WP. DNA nanoswitches: a quantitative platform for gel-based biomolecular interaction analysis. *Nat Meth* 2015, **12**(2)**:** 123-126.

64. Chivers CE, Crozat E, Chu C, Moy VT, Sherratt DJ, Howarth M. A streptavidin variant with slower biotin dissociation and increased mechanostability. *Nat Meth* 2010, **7**(5)**:** 391-393.

65. Neuman KC, Lionnet T, Allemand JF. Single-Molecule Micromanipulation Techniques. *Annual Review of Materials Research* 2007, **37**(1)**:** 33-67.

66. Jeney S, Mor F, Koszali R, Forró L, Moy VT. Monitoring ligand–receptor interactions by photonic force microscopy. *Nanotechnology* 2010, **21**(25)**:** 255102.

67. Rico F, Moy VT. Energy landscape roughness of the streptavidin-biotin interaction. *J Mol Recognit* 2007, **20**(6)**:** 495-501.

68. Teulon J-M, Delcuze Y, Odorico M, Chen S-wW, Parot P, Pellequer J-L. Single and multiple bonds in (strept)avidin–biotin interactions. *Journal of Molecular Recognition* 2011, **24**(3)**:** 490-502.

69. Merkel R, Nassoy P, Leung A, Ritchie K, Evans E. Energy landscapes of receptor-ligand bonds explored with dynamic force spectroscopy. *Nature* 1999, **397**(6714)**:** 50-53.

70. Zhou J, Zhang LZ, Leng YS, Tsao HK, Sheng YJ, Jiang SY. Unbinding of the streptavidin-biotin complex by atomic force microscopy: A hybrid simulation study. *J Chem Phys* 2006, **125**(10)**:** 104905.

71. Walton EB, Lee S, Van Vliet KJ. Extending Bell's model: How force transducer stiffness alters measured unbinding forces and kinetics of molecular complexes. *Biophysical Journal* 2008, **94**(7)**:** 2621-2630.

72. Pincet F, Husson J. The solution to the streptavidin-biotin paradox: The influence of history on the strength of single molecular bonds. *Biophys J* 2005, **89**(6)**:** 4374-4381.

73. Pierres A, Touchard D, Benoliel AM, Bongrand P. Dissecting streptavidin-biotin interaction with a Laminar flow chamber. *Biophysical Journal* 2002, **82**(6)**:** 3214-3223.

74. Guo S, Ray C, Kirkpatrick A, Lad N, Akhremitchev BB. Effects of Multiple-Bond Ruptures on Kinetic Parameters Extracted from Force Spectroscopy Measurements: Revisiting Biotin-Streptavidin Interactions. *Biophysical Journal* 2008, **95**(8)**:** 3964-3976.

75. Dudko OK, Hummer G, Szabo A. Intrinsic rates and activation free energies from single-molecule pulling experiments. *Phys Rev Lett* 2006, **96**(10).

76. Sedlak SM, Bauer MS, Kluger C, Schendel LC, Milles LF, Pippig DA*, et al.* Monodisperse measurement of the biotin-streptavidin interaction strength in a well-defined pulling geometry. *PLOS ONE* 2017, **12**(12)**:** e0188722.

77. Florin EL, Moy VT, Gaub HE. Adhesion Forces Between Individual Ligand-Receptor Pairs. *Science* 1994, **264**(5157)**:** 415-417.

78. Lee GU, Kidwell DA, Colton RJ. Sensing Discrete Streptavidin Biotin Interactions with Atomic-Force Microscopy. *Langmuir* 1994, **10**(2)**:** 354-357.

79. Moy VT, Florin EL, Gaub HE. Intermolecular Forces and Energies Between Ligands and Receptors. *Science* 1994, **266**(5183)**:** 257-259.

80. Izrailev S, Stepaniants S, Balsera M, Oono Y, Schulten K. Molecular dynamics study of unbinding of the avidin-biotin complex. *Biophysical Journal* 1997, **72**(4)**:** 1568-1581.

81. Grubmuller H, Heymann B, Tavan P. Ligand binding: Molecular mechanics calculation of the streptavidin biotin rupture force. *Science* 1996, **271**(5251)**:** 997-999.

82. Hyre DE, Amon LM, Penzotti JE, Le Trong I, Stenkamp RE, Lybrand TP*, et al.* Early mechanistic events in biotin dissociation from streptavidin. *Nat Struct Biol* 2002, **9**(8)**:** 582-585.

83. Freitag S, Chu V, Penzotti JE, Klumb LA, To R, Hyre D*, et al.* A structural snapshot of an intermediate on the streptavidin-biotin dissociation pathway. *Proc Natl Acad Sci U S A* 1999, **96**(15)**:** 8384-8389.

84. Milles LF, Schulten K, Gaub HE, Bernardi RC. Molecular mechanism of extreme mechanostability in a pathogen adhesin. *Science* 2018, **359**(6383)**:** 1527-1533.

85. O'Sullivan VJ, Barrette-Ng I, Hommema E, Hermanson GT, Schofield M, Wu S-C*, et al.* Development of a Tetrameric Streptavidin Mutein with Reversible Biotin Binding Capability: Engineering a Mobile Loop as an Exit Door for Biotin. *PLoS ONE* 2012, **7**(4)**:** e35203.

86. Zhang XH, Moy VT. Cooperative adhesion of ligand-receptor bonds. *Biophys Chem* 2003, **104**(1)**:** 271-278.

87. Bullerjahn JT, Sturm S, Kroy K. Theory of rapid force spectroscopy. *Nat Commun* 2014, **5**.

88. Friddle RW, Noy A, De Yoreo JJ. Interpreting the widespread nonlinear force spectra of intermolecular bonds. *Proceedings of the National Academy of Sciences* 2012, **109**(34)**:** 13573-13578.

89. Cossio P, Hummer G, Szabo A. Kinetic Ductility and Force-Spike Resistance of Proteins from Single-Molecule Force Spectroscopy. *Biophysical Journal* 2016, **111**(4)**:** 832-840.